



Royal Institute of Technology

**Three-dimensional investigation of non-metallic
inclusions during powder metallurgy production**

MH250X

Master of Science Thesis

by

Arkadiy Davydenko

Division of Applied Process Metallurgy
Department of Materials Science and Engineering
KTH Royal Institute of Technology

Stockholm, Sweden (04-2012)

ABSTRACT

Due to growing demands for steel powder properties and continuous evolution of the powder metallurgy (PM) production it is necessary to apply new investigation technics and research applications for quality investigation of the PM products. In addition, it is important to be able to predict the probable maximum size of inclusions.

The industrial scale sampling of steel was made in Höganäs AB. The three dimensional (3D) analysis of non-metallic inclusions obtained by electrolytic extraction (EE) method was applied for metal samples taken from liquid steel before water-atomization and after powder forging process.

It was demonstrated that the application of the 3D analysis has a perspective and possibility to be used independently or like a reference during 2D analysis of inclusions in powder metallurgy products. The tundish samples have the maximum total number of inclusions but have smaller size of complex inclusion. The size range of inclusions in the ladle and tundish samples is between 1 and 46 μm . The main type of inclusions is spherical (Si-Ca-Al-Mg-O in composition). The powder forged samples have two main types of non-metallic particles: “gray” carbon saturated (10-250 μm) and “bright” clustered oxide particles (1-37 μm with Cr-Si-Mn-Mg-Al-O in composition).

The probable maximum size of inclusions was estimated based on a new particle size distribution (PSD) and the standard extreme value distribution (EVD) methods. Both methods predicted that in 1 kg of metal the maximum size of spherical inclusions is $< 15 \mu\text{m}$ in liquid steel samples and the maximum length of “bright” clustered oxide particles is $< 63 \mu\text{m}$ in powder forged samples. However, the prediction of the maximum size by PSD method showed necessity of the further optimization.

ACKNOWLEDGEMENTS

I would like to thank Prof. Pär Jönsson for great opportunity to work at Division of Applied Process Metallurgy and my supervisor Dr. Andrey Karasev for his priceless guidance during my work on this master thesis and for his huge patience with students.

I am grateful to my coordinators in Höganäs AB: Liviu Brabie, Marja Haglund and Ola Bergman for supporting me with everything I needed during my visit to Höganäs AB.

In addition, I am thankful to all my colleagues and friends at Materials Science and Engineering Department, KTH Royal Institute of Technology, Stockholm, Sweden.

Contents

1 INTRODUCTION.....	5
1.1 Powder metallurgy basics.....	5
1.2 Production of metal powder.....	6
1.3 Items production from metal powders.....	9
1.4 Defects and quality in powder metallurgy products.....	9
1.5 The aim of the study.....	11
2 EXPERIMENTAL PROCEDURE.....	12
2.3 Electrolytic extraction.....	12
2.4 Three dimensional investigation of inclusions by SEM.....	16
3 RESULTS AND DISCUSSION.....	17
3.1 Characteristics of inclusions in steel samples from the ladle and tundish (Set 1).....	17
3.1.1 <i>Morphology and frequency of inclusions</i>	17
3.1.2 <i>The number and size of inclusions</i>	19
3.1.3 <i>Prediction of the probable maximum size of inclusions</i>	25
3.2 Characteristic of inclusions in powder forged samples (Set 2).....	29
3.2.1 <i>Morphology of inclusions</i>	29
3.2.2 <i>Number and size of inclusions</i>	29
3.2.3 <i>Prediction of the probable maximum size of inclusions</i>	31
4 CONCLUSIONS.....	33
5 FUTURE WORK SUGGESTIONS.....	34
6 REFERENCES.....	35

1 INTRODUCTION

1.1 Powder metallurgy basics

Nowadays the powder metallurgy (PM) is a complex technology consisting of different processes and steps. The PM industry itself requires relatively low energy inputs, has good yield in material (less machining operations) and can make outputs with good mechanical properties and complicated dimensions. Up till now, the metal powder usage grows rapidly. The modern science and technology have been improving the PM over the years. As a result, the PM has a wide application range: automobile parts (gears, brakes and others), various machining tools, sintered bearings, locks, household equipment, components for electromagnets, filters, print powders, cosmetics and numerous other applications. Some examples of different powder metallurgy products are shown in **Fig. 1**. In simplified way, the PM production process can be divided into several steps:

- 1) metal powder production,
- 2) addition into the metal powder of lubricants,
- 3) compaction of the powder in the special form (die, stamp, etc.),
- 4) heating of the pressed powder in order to reach sintering between metal particles,
- 5) finishing operation (if necessary).

Of course, the PM is not the ideal process and has some drawbacks. Like relatively costly investments in production equipment (furnaces, dies, powder compaction presses and etc.).

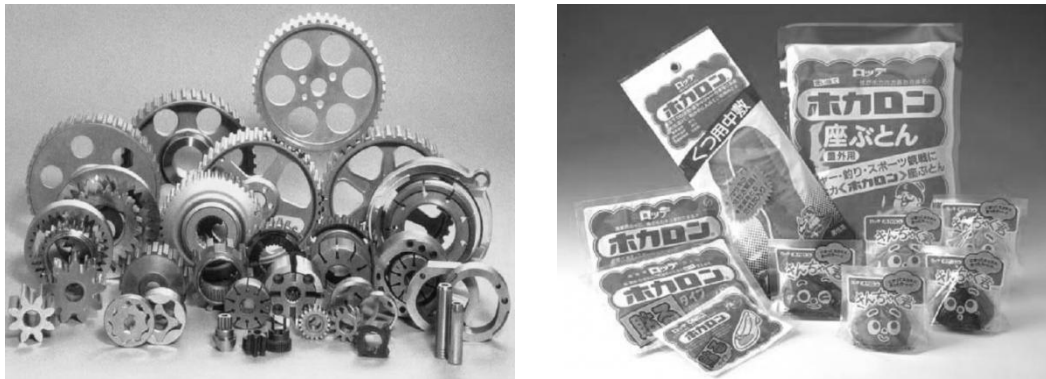


Fig. 1. Some typical components made of metal powder. Mechanical parts on the left side and body warmers on the right [1].

Presence of porosity and voids between metal particles after sintering in final product and thereby difficulties in reaching a “full” density of a material. However, in some cases it is important to have some porosity which can also play a beneficial role like the ability to hold

lubricants better on the product surface, if it is necessary for application (bearings or gears for instance). In spite of continuous development of the PM, the “porosity problem” is still one of the major complications in PM industry.

1.2 Production of metal powder

There are several main technological methods for metal powder production: sponge-iron (known as “Höganäs process”) and water/gas-atomization process. The typical morphology of sponge-iron and atomized powder particles are shown in **Fig. 2**. Some properties of sponge-iron and atomized powder are summarized in **Table 1**.

Table 1. The summary of sponge-iron and atomized powder properties.

Property of a powder	Sponge-iron powder	Atomized powder
Production cost	Low	High
Porosity	High	Low
Compressibility	Low	High
Green strength	High	Low
Mechanical properties of final product made of a powder	Low	High

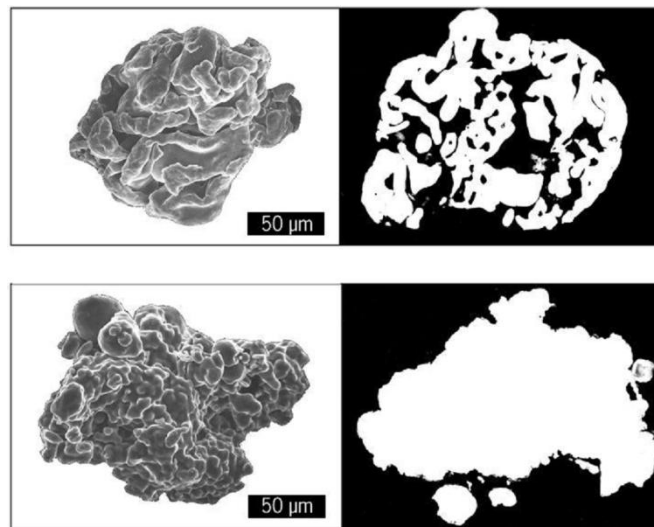


Fig. 2. The typical examples of particles of sponge-iron powder (upper images) and atomized powder (bottom images) [2].

The “Höganäs process” is based on the iron ore reduction. This reduced (under special conditions) iron ore gives a “sponge” product which is subsequently transformed to the powder [2]. Sponge-iron production is cheaper than atomization process and has good green strength (the property of a compacted powder to keep determinated geometry and withstand outside stresses). Usually, the sponge-iron powder is mixed with alloys (powder) mechanically. In this case, the alloying elements can segregate and cause an anisotropy of the mechanical properties in the final product [2].

In atomization process the metal melt stream is dispersed on fine droplets by water or gas jet and the metal powder is produced (**Figs. 3 and 4**). Usually the steel used for atomized powder is produced from melted (in an electric arc furnace) scrap. Before the atomization, the steel is refined in a ladle. Later, the steel is transferred from the ladle to the special tundish. During the steel transition from the tundish, the steel melt is hit by water or gas jet under high pressure. During this water jet “attack” the melt is split on the relative small particles (20-200 μm) [2]. After that, the particles are collected and dried. The moisture free metal powder is separated from impurities like slag, belt, refractory particles. Since the water is being used, the steel powder is oxidized drastically. Moreover, due to water atomization environment conditions (the fast cooling rate) the metal particles are eventually hardened. These powder’s features are not desirable and the metal powder is annealed later on in order to reduce oxides on the powder surface and residual carbon inside the powder core [2]. After, the powder is mixed with alloys (if necessary), homogenized, checked by quality control and packed.

The atomized powder is easy to press and it can be alloyed before atomization [3]. In addition, the atomized powder has less inner pores. Adding of alloys before the atomization yields the homogenous distribution of alloys in the powder grains and in the final product as well. Thereby, alloying of melt before atomization allows to produce the products with better mechanical properties.

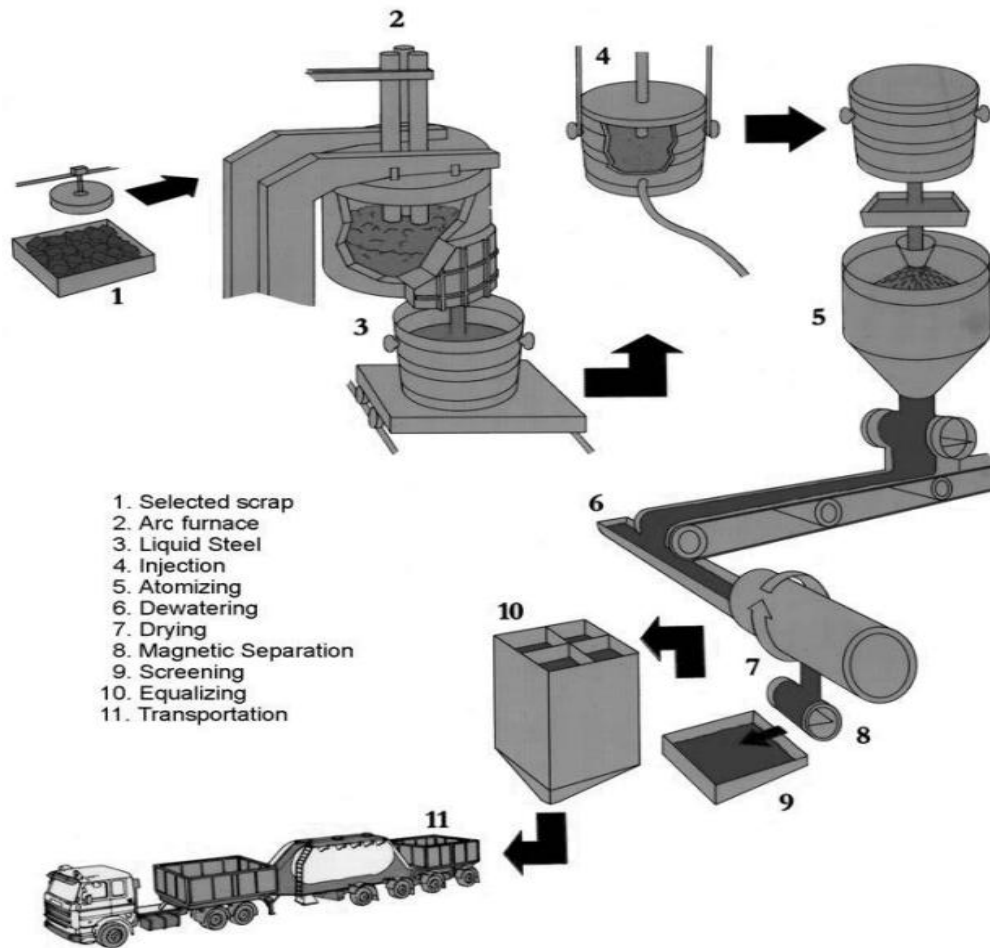


Fig. 3. The water-atomized powder production route in Höganäs AB [2].

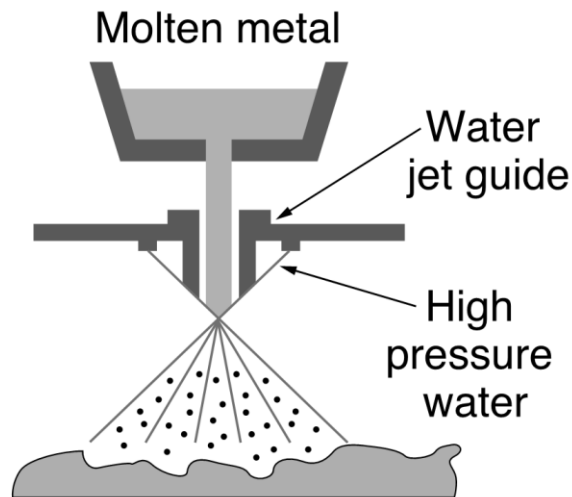


Fig. 4. The scheme of liquid steel water-atomization [1].

1.3 Items production from metal powders

The components produced from metal powders are made in several steps: mixing, pressing, sintering and machining with heat treatment if necessary. Required alloys (like graphite and other alloying powders) can be added during the powder mixing. Lubricants are added in order to make easier the compaction operation. After the powder has filled the special designed die, the powder is pressed. The metal powder compaction with some technical improvements such a powder forging (PF) process (**Fig. 5**) allows to reach almost the “full” density in a final product by the addition of an extra “compaction/forging” step (pressing under evaluated temperatures). During the sintering, the lubricants are burnt out and the metal powder particles are bound between each other.

As it was mentioned earlier, one the major drawbacks of PM is porosity. The PF technique has helped the PM industry to mitigate this problem. After PF process there is only residual porosity [4]. However, this porosity problem still does not allow to assert that the PF products have the same properties as the metals.

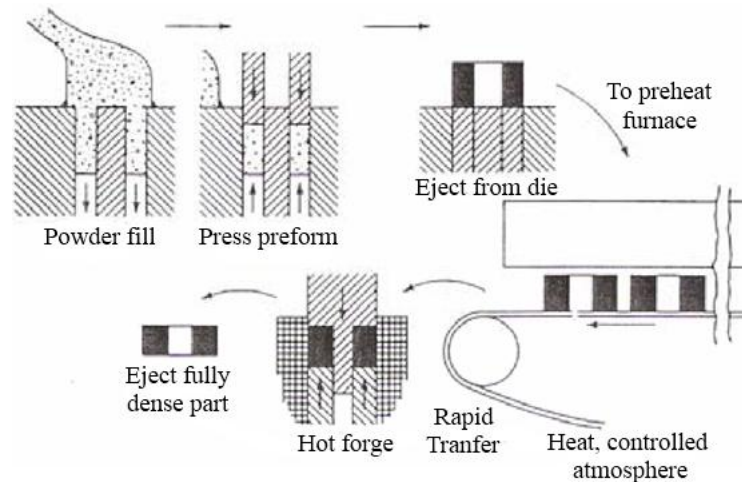


Fig. 5. The schematic illustration of powder forging process [4].

1.4 Defects and quality in powder metallurgy products

The PM production includes different process such as heat-transfer, gas- and hydrodynamic, numerous chemical reactions, phase transformation and etc. As a result, the metal powder can have several types of defects [5]:

- 1) oxidized surface on the powder particles with non-uniform thickness around the powder grains [6],
- 2) slag and non-metallic inclusions which can be located around and/or within the powder grains,
- 3) holes or cavities which can provoke/initiate the crack formation.

Nowadays, a pore size is relatively equal to the size of non-metallic inclusions or even smaller. This was achieved by the evolution of the PM industry with the help of PF technology. Thereby, the inclusions have started to play more harmful role than pores in the PM final products [4].

It is known that the non-metallic inclusions are one of the top problems in modern metallurgy. Inclusions (oxides, sulfides, nitrides and etc.) usually are formed at the deoxidation step during steel making process. Along the steel route before atomization, it is assumed that most of the inclusions are removed during the ladle and tundish treatment. However, these steps do not guarantee 100% steel purity. Inclusion keep to form during reoxidation of the steel melt and not all impurities are removed during gas blowing and/or slag treatment and thereby they could be involved in final PM products after atomization of liquid steel.

Inclusions may cause negative effect on final product properties (fatigue life, machinability, ductility and etc.) [7]. Decades of research have assisted engineers to decrease the number and size of inclusions. After all, the purity of metal is still a big challenge. Since the powder properties depend on steel quality from which it is produced, it is very important to control characteristics of inclusions (number and size for instance) during the whole PM production processes [4] in order to minimize a probable failure and to manufacture high quality products.

During alloying of the metal melt (before atomization), the additions of some alloys (like Mn and Cr) must be well controlled because these additions lead to oxide products formation within the steel melt, particularly during the water-atomization process.

It has been found that different aspects of inclusions influence on PM products. Dogant [8] found that the crack formation was dependent on position of inclusions (commonly on the material's surface) in the steel matrix. And it was observed that clustered oxides were usually the sources of fractures. The nonmetallic particles form micro-cracks and can cause voids formation around themselves, thereby, affect the material properties [8]. Powder compaction punch properties deteriorate under the load because of the cracks caused by the presence of inclusions in the powder [9]. In addition, inclusions can affect a PM products lifetime [2].

The non-metallic inclusions in PM products are usually investigated by two-dimensional (2D) observation on the polished cross section of a steel specimen. The 2D observation method can provide useful information about location, morphology and composition of inclusions in the steel matrix. The 2D analysis is comparatively cheap and not time consuming (often the 2D method is used along with special computer software which allows to decrease time for analysis and increase efficiency of the studying). On the other hand, it has problems with investigation of the real size of inclusions, real morphology and it is quite difficult to distinguish clustered inclusions

within analyzed area/volume. The non-metallic particles (**Fig. 6**) may have “separated” morphology which in return, impedes the 2D analysis or/and decreases the obtained data reliability. The 2D image analysis uses the concept of “near neighbor” separation and Feret’s diameter (**Fig. 7**). This concept can categorize a single inclusion like separate particles

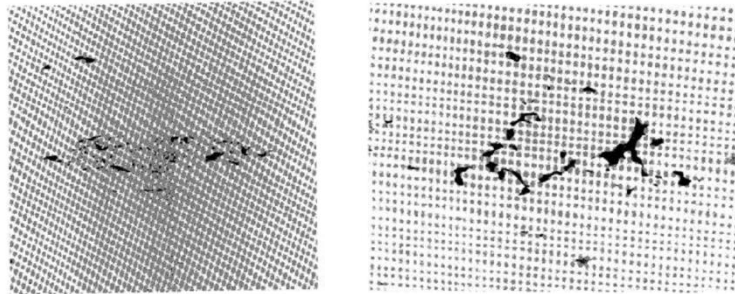


Fig. 6. The cross section images of oxide inclusion (left side) and slag inclusion (right side) [10].

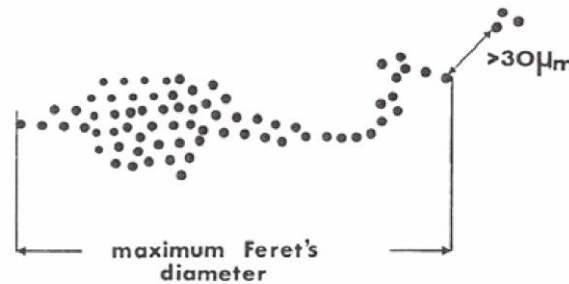


Fig. 7. The concept of “near neighbor” separation and Feret’s diameter [10].

or count several inclusions like one single particle. Moreover, presence of small pores can be counted like inclusions since the pores color on the screen is close to non-metallic particles color [4]. So, it is very difficult to obtain the real data even with visual manual quantitative investigation.

1.5 The aim of the study

The aims of this study are following:

- 1) Investigate characteristics of non-metallic inclusions during modern PM production route.
- 2) Apply a three-dimensional (3D) analysis of inclusions method after electrolytic extraction (EE) by using scanning electron microscope (SEM).
- 3) Estimate the probable maximum size of inclusions in the steel samples taken before water-atomization and in the powder forged products.

2 EXPERIMENTAL PROCEDURE

The sampling procedure was made in industrial trial in Höganäs AB company (Sweden). The first set of samples were taken from the steel melt before the water-atomization stage (**Fig. 8**). The sampling was made during casting of one heat directly from the melt stream after the ladle (L) and tundish (T). Lollipop samples were taken at 10, 40 and 70 min after the beginning of casting (Set 1). The second set (Set 2) of samples was taken from forged powder in different lots. Before forging the steel powder was annealed and mixed with 0.5 wt% graphite (flakes). The specimens for electrolytic extraction were cut from the middle of cylinder forged at 1120°C.

All samples were cut in rectangular shape and EE was applied for each sample. After filtration, inclusions were analyzed on the film-filter by SEM.

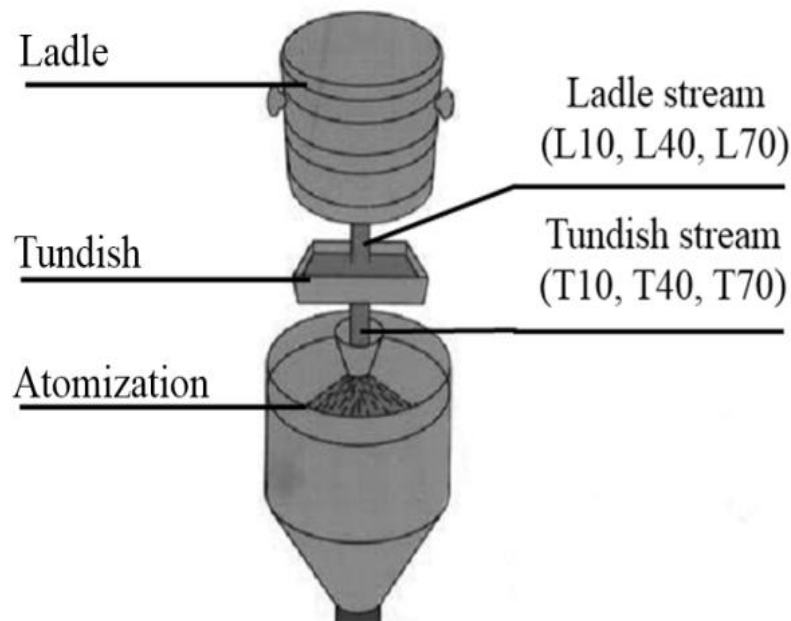


Fig. 8. The sampling of the liquid steel before atomization.

2.3 Electrolytic extraction

The 3D investigation of inclusions characteristics in the steel samples were carried out by scanning electron microscopy (SEM) after electrolytic extraction (EE) of metal specimens. Based on the obtained data it is possible to get reliable particle size distribution (PSD), composition and morphology of non-metallic particles.

The specimens for electrolytic extraction had dimensions presented in **Fig. 9**.

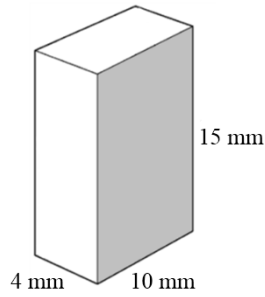


Fig. 9. The geometry of the a specimen (for L/T and PF samples) before extraction.
The grey area represents a side dissolved by EE method.

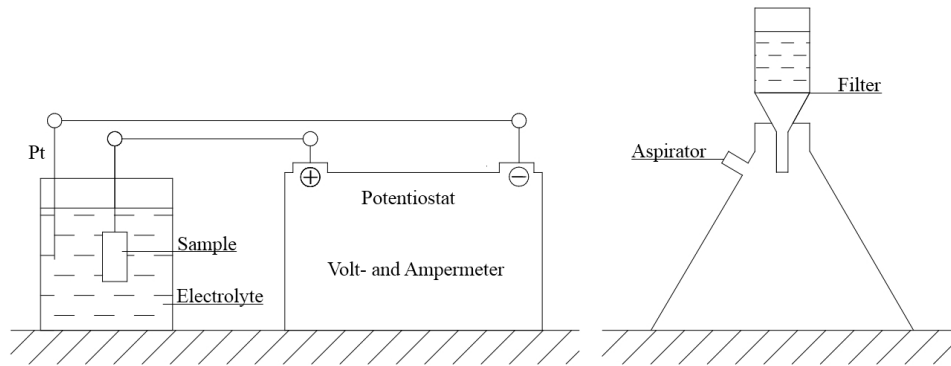


Fig. 10. The schematic illustration of electrolytic extraction process and filtration of solution with extracted inclusions.

The EE method is based on dissolution of metal matrix in electrolyte by applying electric current (**Fig. 10**). The EE process extracts the non-metallic particles from metal specimens. After the extraction, the electrolyte with inclusions is filtered. By applying different extraction settings (electric charge) it is possible to reach the desirable depth of dissolved layer of the metal specimens.

Before EE, all specimens were treated in ultrasonic bath and then cleaned by acetone and petroleum benzene. The weight of steel specimens was measured before and after extraction in order to determine the volume of dissolved metal. All samples were dissolved by potentiostatic electrolytic extraction method in 10% acetylacetone-1% tetramethylammonium chloride-methanol solution (10%AA electrolyte).

In order to be able to investigate inclusions with the largest possible size it is important to dissolve by EE good enough layer of a metal specimen by different settings application during extraction process. In this study, the 3D investigations of inclusions on film-filter by SEM showed the significant difference between film-filters of the L/T and PF samples depending on applied electric charge during extraction process. The several SEM images of non-metallic

inclusions and unidentified precipitation on film-filter surfaces after EE of L40 and PF5 samples after EE at different electric charges are demonstrated in **Fig. 11**. As can be seen in **Fig. 11(a)** and **(b)**, L40 sample extracted at 1500C and 800C electric charge did not show significant difference in appearance and demonstrated possibility to distinguish inclusions with size larger than 1 μm . The amount of C-compound precipitation in these cases is satisfactorily small. On the other hand, **Fig. 11(c)** and **(d)** demonstrates the results for PF5 samples obtained at 800C and 500C respectively. At the 800C electric charge the inclusions investigation was impossible or impeded by unidentified precipitation on the film-filter surface. Probable explanation for this precipitation is suggested in Sec. 3.2.2. Therefore, the electric charge for extraction of PF samples was decreased till 500C which is significantly lower in comparison with the extraction of L/T samples. As can be seen in **Fig. 11(d)** it was possible to distinguish inclusions by using 500C for EE of PF samples. Since details about these phenomenon and/or reasons of limitation are not clear today, more further investigation is required.

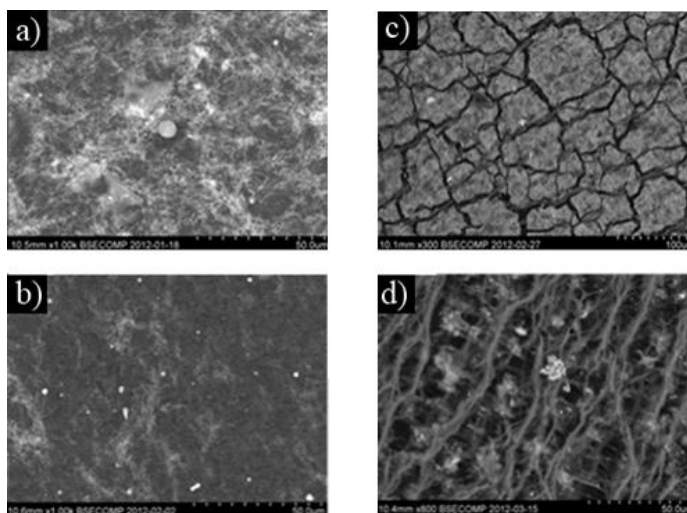
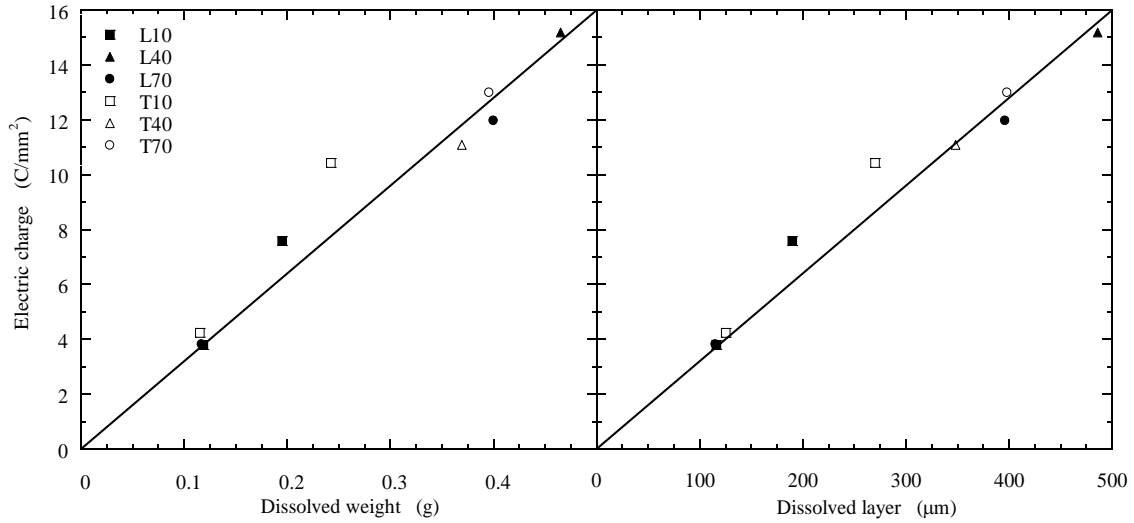
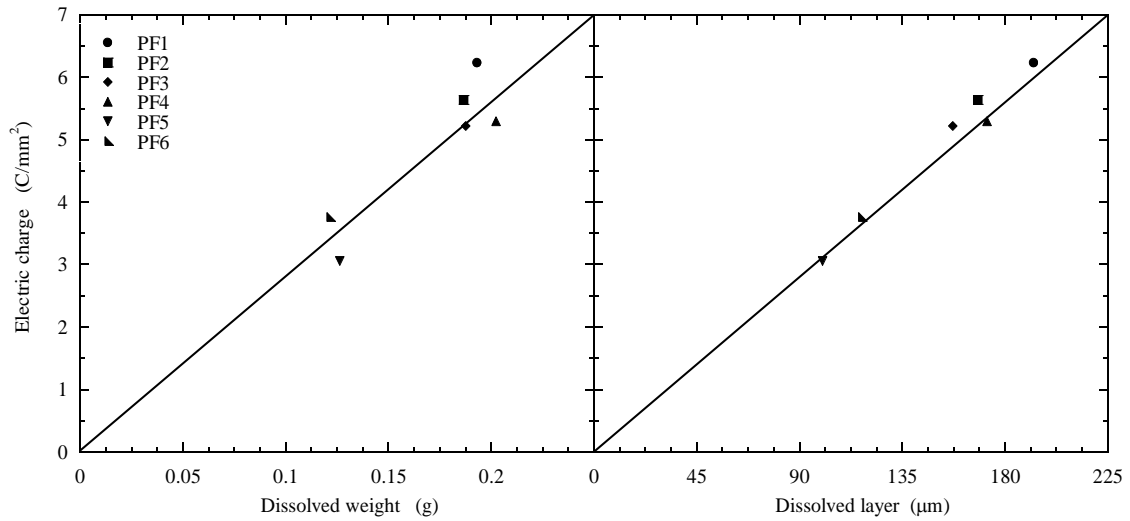


Fig. 11. The typical SEM images for: a) L40 (1500C), b) L40 (800C), c) PF5 (800C) d) PF5 (500C).

During extraction the following parameters were used: 500-1850 Coulombs electric charge, 3.2-4.0 V voltage, 30-63 mA electric current. Additional characteristics of EE are given in **Table 2**, **Figs. 12** and **13**. The archived depth of dissolved layer allows to observe inclusions from $\sim 1 \mu\text{m}$ to $\sim 480 \mu\text{m}$ in size.

Table 2. EE information for L/T and PF samples.

EE parameters	L/T (set 1)	PF (set 2)
Electrolyte	10%AA	10%AA
Dissolved weight (g)	~0.195-0.465	~0.123-0.202
Dissolved layer (μm)	~190-486	~98-192
Filter type	PC-0.4 μm	PTFE-3.0 μm

**Fig. 11.** The relationship between applied electric charge, dissolved weigh and layer in L/T samples.**Fig. 12.** The relationship between applied electric charge, dissolved weigh and layer in PF samples.

The filtration of the solution with extracted non-metallic particles was carried out by using of polycarbonate membrane (PC) film-filter with an open-pore size 0.4 μm for L/T samples and polytetrafluoroethylene (PTFE) film-filter with an open-pore size 3.0 μm for PF samples. The PTFE filter was used in order to decrease the influence of carbon content in the filter matrix on

composition analysis of particles in PF samples. After filtration a part of filter with non-metallic inclusions were used for SEM observation.

2.4 Three dimensional investigation of inclusions by SEM

For 3D investigation of non-metallic inclusions on surface of a film filter was carried out by using the S3700N Hitachi SEM (20 kV and 10 mm working distance) with the back scattered electrons (BSE) signal. The chemical composition of inclusions was analyzed with energy dispersed spectrometry (EDS).

In order to estimate the homogeneity of inclusions distribution on film-filter the filter surface was divided into several zones: top (center of a film-filter), middle and bottom (close to filtration area boundary) (**Fig. 13**). For each zone 15 pictures were made at 400 and 1000 magnifications for L/T samples and at 200 and 500 magnifications for PF samples. The magnification settings were chosen in order to observe large enough filter area (at lower magnification) accompanying with high measurement accuracy. Since the particles were in different size ranges it was decided to apply different magnification for each set of samples in order to increase the data reliability.

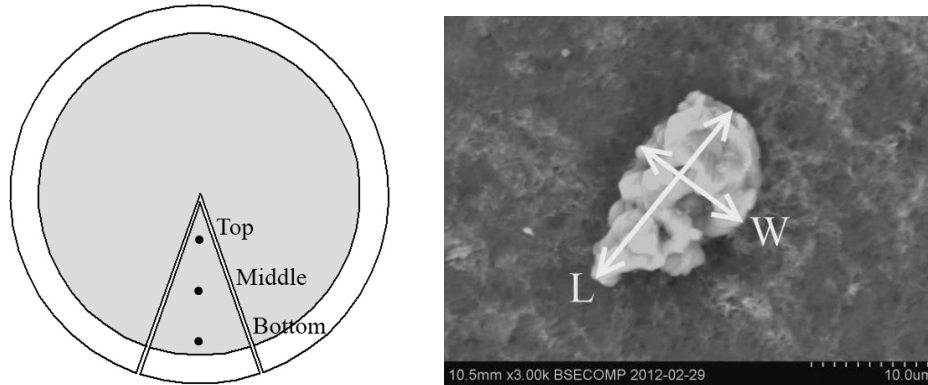


Fig. 13. The observation zones on film-filter (on the left) and the principle of inclusion size estimation (length and width) in the 3D and EE method (on the right).

When SEM images were taken, the measurement of inclusion size (L-length and W-width) was made manually, as shown in **Fig. 13**. For spherical particles the equivalent diameter was calculated.

For determination of PSD the Eq. (1) was used.

$$N_V(i) = \frac{n(i) \times A_{fil} \times \rho_{Me}}{A_{obs} \times W_{dis}} \quad (1)$$

Where $N_{v(i)}$ is the total number of particles per unit value; $n_{(i)}$ is the number of particles in size range “ i ” size range; A_{fil} is the total filtration area; ρ_{Me} is the metal density ($\sim 0.0078 \text{ g/mm}^3$); A_{obs} is the observed area on the filter and W_{dis} is dissolved weight of the metal specimen.

3 RESULTS AND DISCUSSION

3.1 Characteristics of inclusions in steel samples from the ladle and tundish (Set 1)

3.1.1 Morphology and frequency of inclusions

The typical observed inclusions in steel samples from the ladle and tundish (L/T samples) are shown in the **Table 3**. The decided groups are (by decreasing in frequency order): spherical, elongated, regular (and irregular) and complex. The frequency of inclusions with different morphology in L/T samples depending on the sampling time is shown in **Fig. 14**.

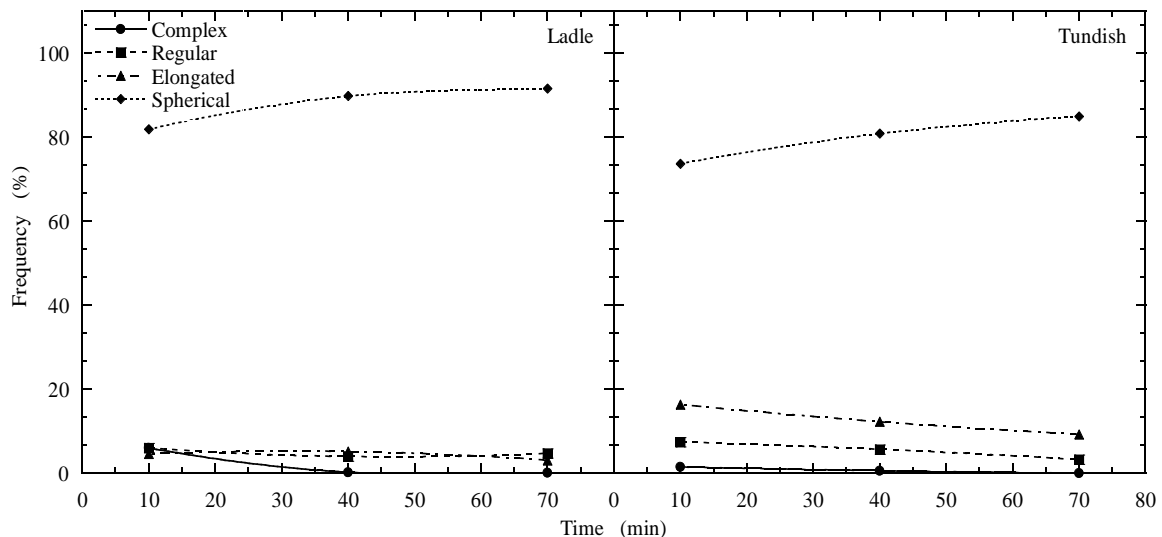
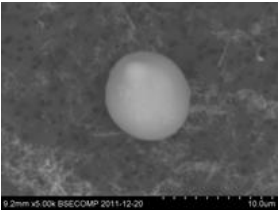

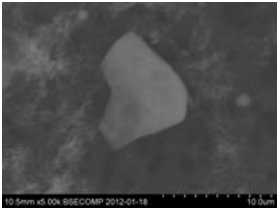
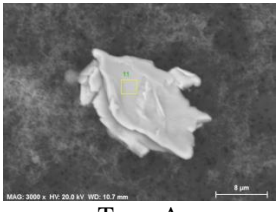



Fig. 14. The frequency of inclusions in L/T samples.

The spherical particles are the most frequent ($\sim 74\text{-}92\%$) in L/T samples. The frequency of spherical inclusions grows slightly (on $\sim 10\text{-}12\%$) with time due to reoxidation (open ladle stream) of the steel melt during casting. According to the morphology of spherical particles, it can be assumed that inclusions are liquid in the steel melt during casting process. The total frequency of spherical inclusions in the tundish samples is lower approximately for 7-9% compared to the ladle samples.

The elongated inclusions are the second most frequent ($\sim 3\text{-}17\%$) non-metallic particles in L/T samples. The frequency variation of elongated does not change in the ladle samples and slightly decreases in the tundish samples approximately from 10% to 17%.

Table 3. The typical morphology and composition of inclusions in L/T samples.

Inclusion type	Image	Size and length range (μm)	Chemical composition	Frequency of inclusions (%)
Spherical (SP)		$0.7 \leq d_v \leq 17$	Si-Ca-Al-Mg-O	~74-92
Elongated (EL)		$2 \leq L \leq 20$	Ca-Mg-Si-Al-O+MnS	~3-17
Regular and irregular (RE and IR)		$1 \leq L \leq 46$	Si-Na-Mg-Ca-Al-O	~3-8
Complex (COM)	 Type-A	$4 \leq L \leq 25$	Fe-Cr-Ni-Si-Mn-O	~0-6
	 Type-B	$2 \leq L \leq 20$	Ca-P-Mg-Al-O	

The overall frequency of elongated particles in the tundish samples is larger (on ~6-12%) than in the ladle samples. The probable reason for the increased frequency of elongated inclusions in the tundish samples is a collision of spherical particles between each other caused by turbulence (ladle stream) during the steel casting into the tundish. The lowered frequency of spherical particles in the tundish speaks favorably in support of the previous statement.

The regular (and irregular) particles are the third most frequent (~3-8%) inclusions in L/T samples. Based on the morphology of regular particles, it can be concluded that these inclusions could be in solid phase during casting process. The frequency variation of regular inclusions almost does not change during the whole casting process.

The complex inclusions have the smallest frequency (~0-6%) with stable decreasing tendency. The decreasing temperature during casting (~1°C per 1 min according to operators in the melt shop) can influence the shape and frequency of complex inclusions. In order to have the lowest content of complex inclusions in the steel product the best period for steel production is after 40 min from the beginning of the casting.

3.1.2 The number and size of inclusions

Regular inclusions

The regular (RE) inclusions are not the most frequent but this type of inclusions has the largest value of L_{\max} (up to 46 μm). The composition of regular particles varies in following range (in mass %): 50-88% SiO_2 , 0-44% Na_2O , 1-43% MgO , 2-28% CaO , and 0-8% Al_2O_3 . Elements like Na_2O and MgO could come from the tundish powder and refractory.

The number and average length of RE particles in the L/T samples depending on the sampling time is shown in **Fig. 15**. It can be seen that the total number of RE particles per unit volume ($T. N_v$) significantly decreases (on ~57%) in the ladle samples and obviously increases (on ~87%) in the tundish samples during casting. A peak of $T. N_v$ value of RE inclusions in the T40 tundish sample could be caused by sampling problems. In the ladle there is low reoxidation favorable for inclusions growing and likely the slag treatment decreases the number of inclusions. On the other hand, the probable reasons for increasing $T. N_v$ value in the tundish are following: the slag and refractory capturing by the ladle stream and high reoxidation (open ladle stream) of the melt. The average length of RE particles in the ladle samples is relatively large at the beginning (L10) of the casting process and becomes lower (on ~50%) at the end (L70) of the casting process. Though the maximum length of RE inclusions observed in the ladle samples was ~46 μm the average length of these inclusions is about 4 μm . In the beginning of the process in the ladle large reoxidation of the steel melt could be accompanied by flushing into the steel melt exogenous particles like refractory, slag and etc. This might explain the peak in size at the

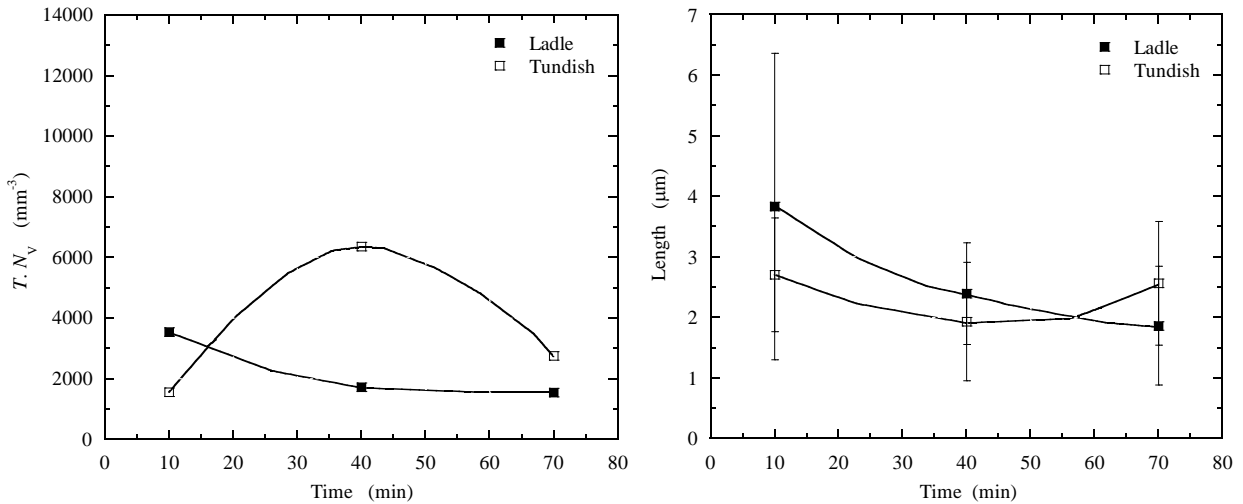


Fig. 15. The total number (left side) and average length (right side) of regular inclusions in L/T samples.

beginning of the casting process for the ladle stream. In the tundish the average length of RE inclusions does not change significantly and varies from ~ 2 to $\sim 2.7 \mu\text{m}$ during the whole casting process. Since the RE inclusions are significantly smaller in size after 40 min, the melt has been casted after 40 min is more suitable for production of steel with smaller regular inclusions. However, the number of these inclusions in the T40 and T70 samples is considerably higher in comparison with T10 sample.

Complex inclusions

The complex (COM) inclusions are the second largest (L_{max} up to $\sim 25 \mu\text{m}$) non-metallic particles in L/T samples. Basically, the group consists of two particle sub-types (A and B) distinguished by morphology and chemical composition (**Table 4**). The composition of the largest ($\sim 4\text{-}25 \mu\text{m}$) type-A COM inclusions varies in following range (in wt. %): 27-51 % Fe, 11-21% Cr, 8-18% Ni, 2% Si, 2% Mn. Type-A particles could be a product of not dissolved ferro-alloys added into the steel melt. Anyway, type-A inclusions are not typical for liquid steel and the source of these particles is unclear. In order to obtain more details about type-A COM inclusions more investigation is required. The composition of the second largest type-B COM particles ($\sim 2\text{-}20 \mu\text{m}$) varies in the range (in mass %): 48-54% CaO, 46-52% P_2O_5 , 0-2% MgO, 0-1% Al_2O_3 . Type-B inclusions are also not typical for liquid steel and the source of these particles is unknown as well. In order to obtain more details about type-B COM inclusions additional investigation is needed. The number and average length of COM particles in the L/T samples depending on the sampling time is shown in **Fig. 16**. It can be seen that the total number of COM particles per unit volume ($T.N_v$) in the L/T samples is the largest in initial period of casting and

decreases drastically during the casting. Probably, some inclusions assimilate into the slag or dissolve in the

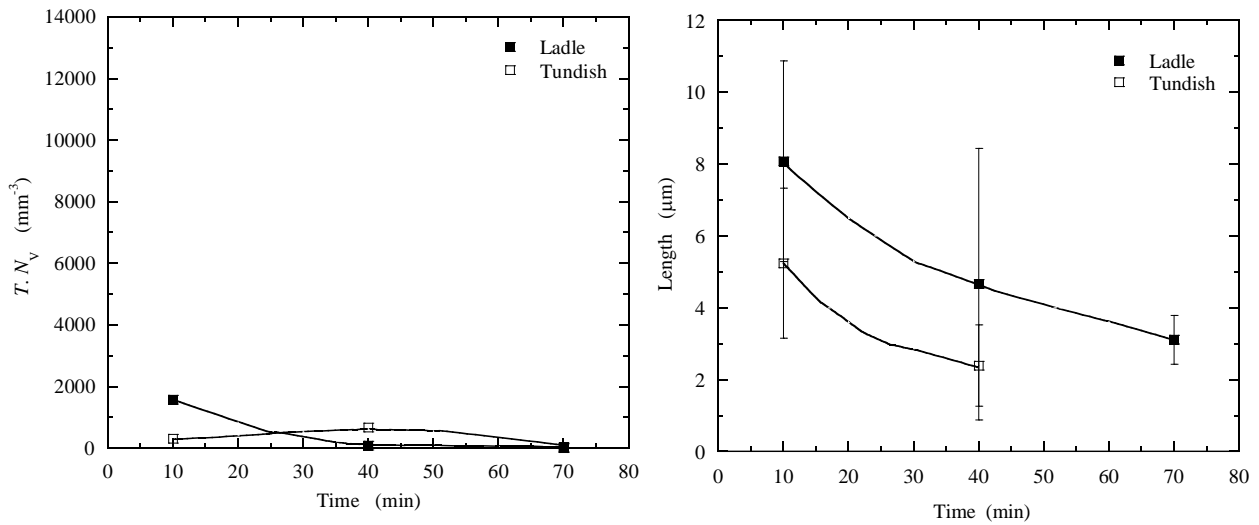


Fig. 16. The total number (left side) and average length (right side) of complex inclusions in L/T samples.

steel melt during casting process and thereby these inclusions decrease in the number. The average length of COM inclusions shows the similar decreasing tendencies in the L/T samples. Namely, the average length is relatively large at the beginning ($\sim 8 \mu\text{m}$ in L10) of the casting process and becomes lower (on $\sim 63\%$) at the end ($\sim 3 \mu\text{m}$ in L70) of casting. The average length of complex inclusions in T10 sample ($\sim 5 \mu\text{m}$) is $\sim 50\%$ larger than in T40 sample ($\sim 2.5 \mu\text{m}$). In the sample T70 no complex inclusions were observed. The casting after 40 min is more convenient for production of steel with lower number ($< 3\%$) and smaller size ($< 5 \mu\text{m}$) of complex particles.

Elongated inclusions

The elongated (EL) inclusions are the third largest (L_{max} up to $20 \mu\text{m}$) type of non-metallic particles. The composition of EL inclusions varies in following range (in mass %): 0-54% CaO, 5-53% MgO, 0-48% SiO_2 , 21-38% Al_2O_3 and the rest 0-21% MnS. One of the main probable reasons for EL inclusions formation is collision of liquid spherical particles between each other caused by turbulence (ladle stream) during the steel casting. In addition, a heterogeneous precipitation of MnS on oxide inclusions during cooling and solidification of steel samples may be another reason for EL inclusions formation.

The number and average length of EL particles in the L/T samples depending on the sampling time is showed **Fig. 17**. The total number of EL particles per unit volume ($T.N_v$) clearly decreases (on $\sim 50\%$) in the ladle samples and considerably grows (for $\sim 136\%$) in the tundish

samples. A peak of $T. N_v$ value of EL inclusions in the T40 tundish sample might be caused by sampling problems. In the ladle there is low reoxidation and thereby stable $T. N_v$. On the other hand, other theoretical reasons for increasing $T. N_v$ value in the tundish could be: the collision of inclusions due to turbulence and strong melt reoxidation (open ladle stream). The

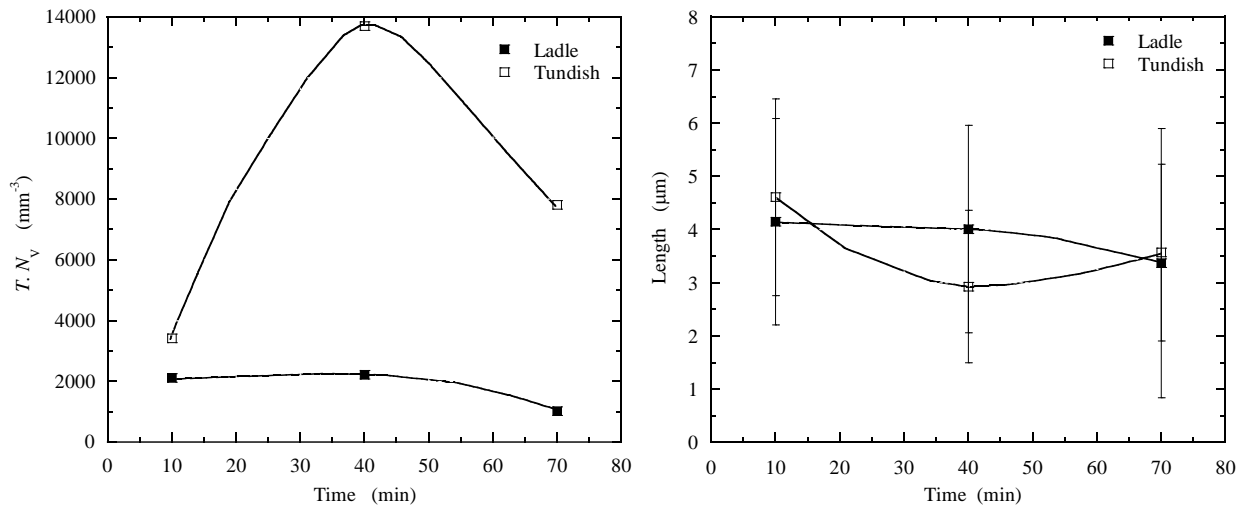


Fig. 17. The total number (left side) and average length (right side) of elongated inclusions in L/T samples.

average length of EL inclusions shows the similar decreasing tendencies in the L/T samples. Viz, the average length of EL particles decreases (on average $\sim 22\%$) in the L/T samples from $\sim 4.2/4.6$ to $\sim 3.3/3.5$ μm respectively. The turbulence and reoxidation in tundish, should be avoided in order to decrease the number of elongated particles.

Spherical inclusions

The spherical (SP) inclusions are the typical non-metallic particles (the maximum size up to ~ 17 μm) in L/T samples. The composition of SP inclusions varies in following range (in mass %): 30-66% SiO_2 , 5-38% CaO , 19-25% Al_2O_3 , 5-8% MgO . Taking in account the composition of SP inclusions, it is possible to assume these particles are reoxidation products. The composition range of SP non-metallic particles depending on the size is shown in **Fig. 18**. It can be seen that in the size range from ~ 1.7 to ~ 8.2 μm the SiO_2 content decreases from ~ 66 to $\sim 29\%$, CaO content increases from ~ 5 to $\sim 38\%$, Al_2O_3 content is stable and MgO grows from ~ 3 to 8%. It is possible to conclude that SP inclusions larger than 6 μm are stable in composition. The number of SP particles in size range smaller and larger than 2 μm in the L/T samples depending on the sampling time is shown in **Fig. 19**. The total number of small SP particles (< 2 μm) per unit volume ($T. N_v$) grows in the ladle samples from ~ 29000 to ~ 57000 mm^{-3} and from ~ 35000 to ~ 85000 mm^{-3} in the tundish samples. It can be seen that the $T. N_v$ values of smaller SP particles in initial moment (L10 and T10 samples) are similar. However, the number of these particles in

the tundish increases drastically with casting time in comparisons with that in the ladle samples. A peak of $T. N_v$ value of SP inclusions in T40 sample might be caused by sampling problems. The growing $T. N_v$ of smaller SP inclusions can be caused by reoxidation processes during casting (open ladle stream). At the same time, the $T. N_v$ of large SP particles ($> 2 \mu\text{m}$) accompanied by low/high

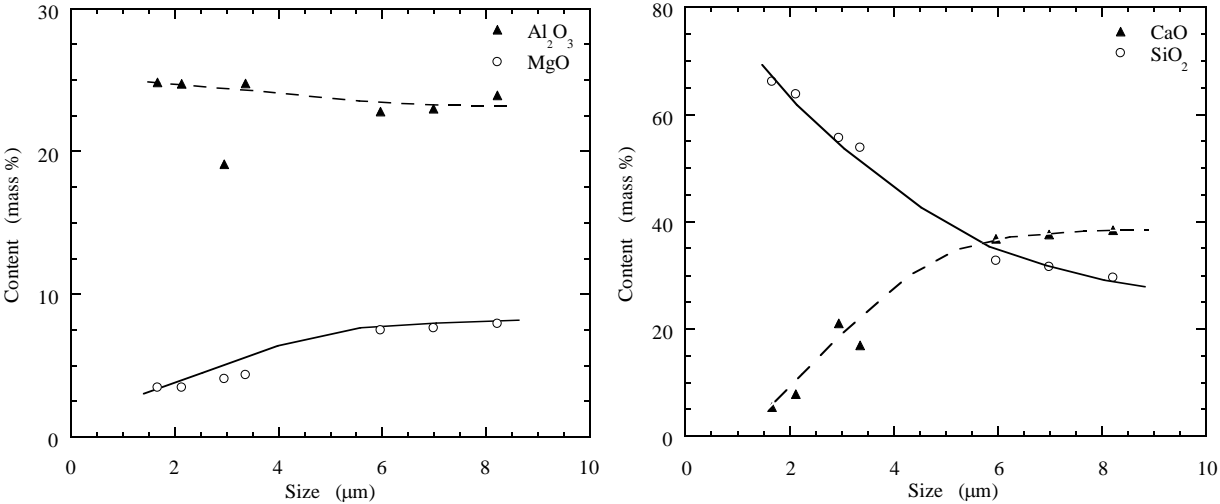


Fig. 18. The chemical composition of spherical inclusions in L/T samples.

reoxidation in the ladle/tundish respectively does not change significantly in L/T samples. The average size of large SP inclusions in the L/T samples does not change significantly and stays in the size range 2.5-2.7 μm under the whole casting process, as it is shown in Fig. 20.

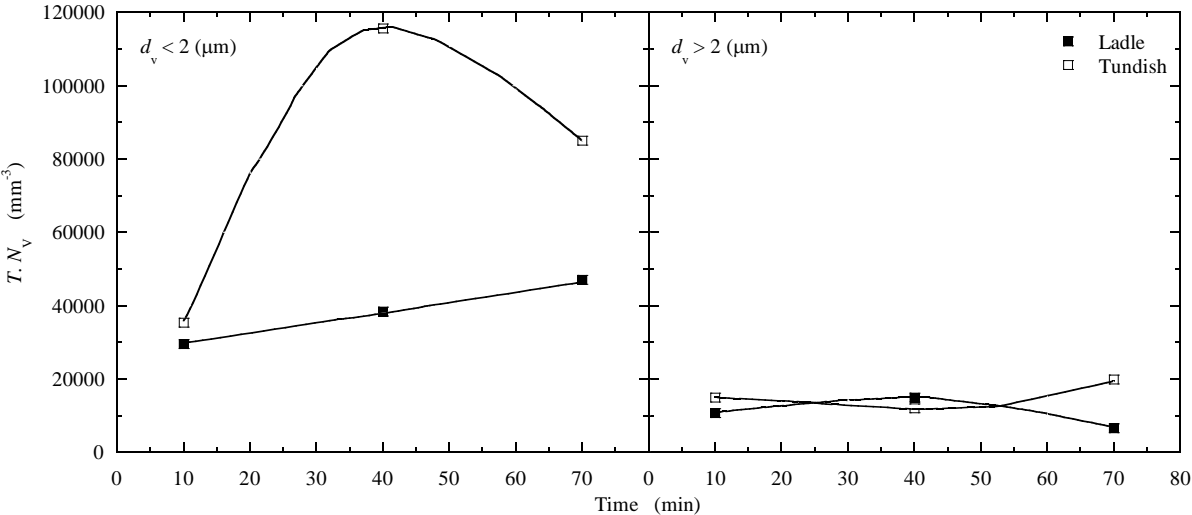


Fig. 19. The total number of spherical particles with size smaller and larger than 2 μm on the left and right side respectively in L/T samples.

The highest frequency of SP inclusions in L/T samples made it possible to estimate the reliable particles size distribution (PSD) of these non-metallic particles. In order to estimate PSD for SP inclusions in L10 sample three zones (top, middle, bottom) were observed by SEM. The comparison of PSD for each zones showed good correlation between each other. This allowed to assume that the SP inclusions are homogeneously distributed on the film-filter surface. Based on this it was

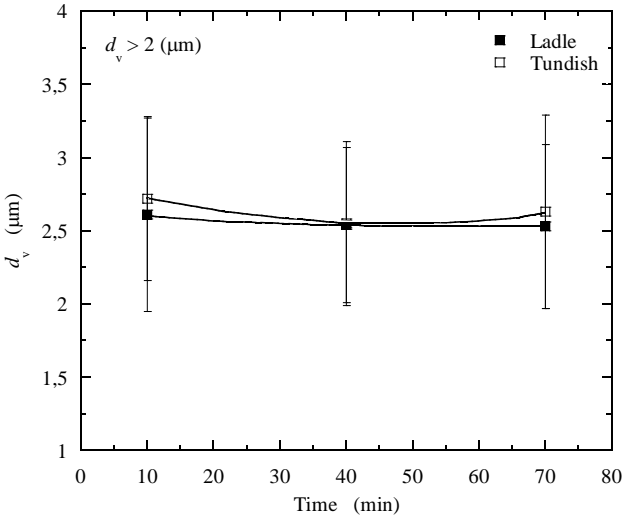


Fig. 20. The average size of spherical inclusions in L/T samples.

decided to study only the top and bottom zones for PSD estimation in all samples. The PSD for different observation zones in L10 and T10 samples is shown in **Fig. 21**. As can be seen, the PSD correlates well for all observation zones in L10 and T10 samples. The PSD for all zones in L10 and T10 samples correlate well between each other. Thereby, it was reasonable to conclude that the

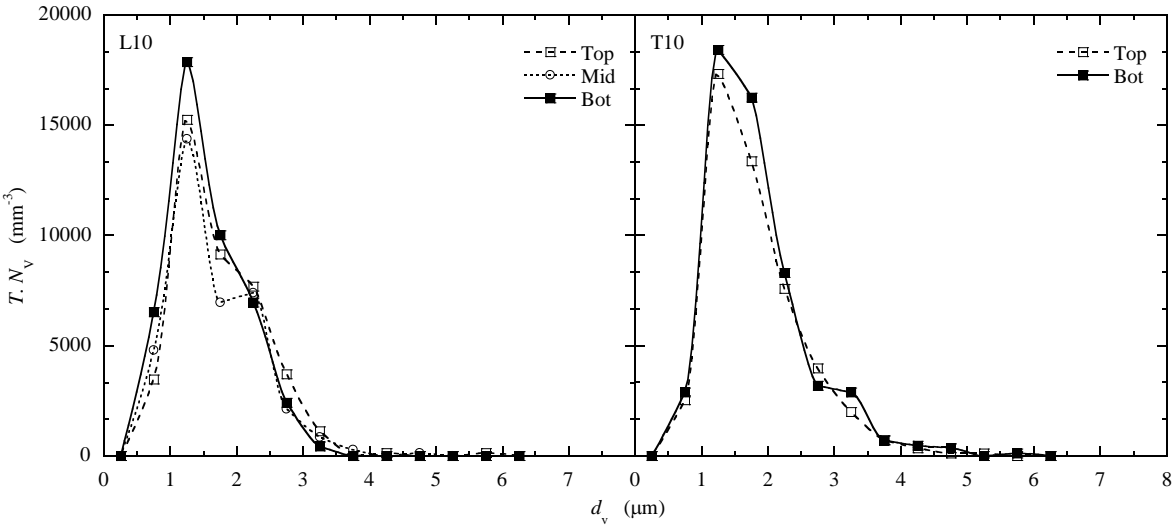


Fig. 21. The comparison of PSD in L10 and T10 samples for different zones of film-filters.

estimation of PSD based on the data obtained in top and bottom zones can provide the reliable data. The PSD (0.5 μm size step) for spherical inclusions in L/T samples is showed **Fig. 22**. All samples have the top of PSD in the range $< 2 \mu\text{m}$. The highest peak value of $T.N_v$ corresponds to the T40 sample (likely due to the sampling problems). The difference in PSD for small SP inclusions ($< 2 \mu\text{m}$) in L/T samples mostly could be caused by different reoxidation conditions (open melt stream, slag capturing in the tundish and etc.) during the casting process. In the range $> 2 \mu\text{m}$, the PSD for SP inclusions is similar to each other in L/T samples.

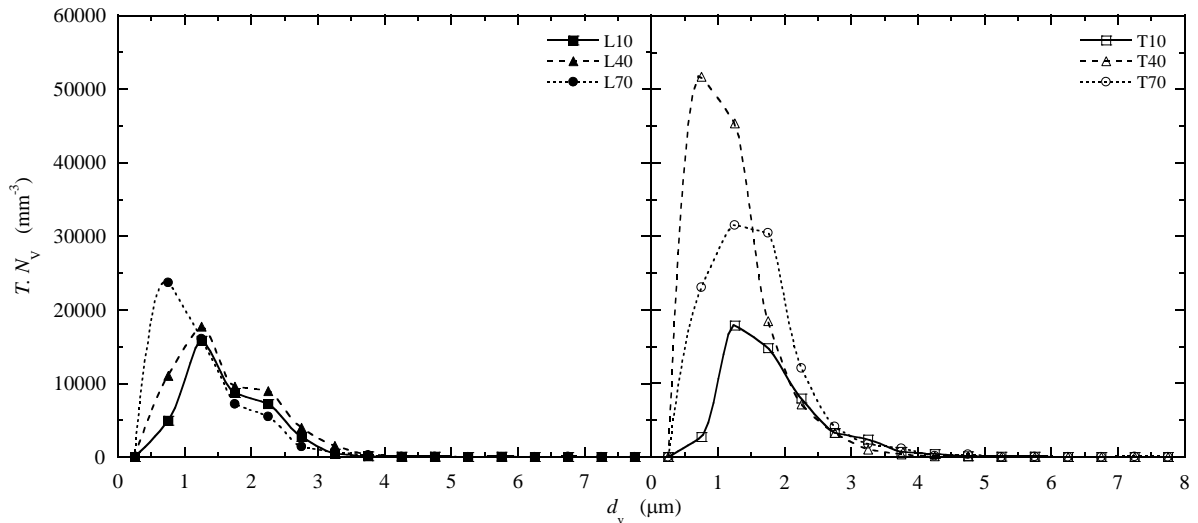


Fig. 22. The particle size distribution of spherical inclusions in L/T samples.

In order to decrease the number of small spherical particles the reoxidation of the melt during casting should be avoided.

3.1.3 Prediction of the probable maximum size of inclusions

Since one of the major dangerous factors of non-metallic inclusion is the size of a harmful particle it is important to be able to predict the probable maximum size of inclusion. One of the useful standard methods for a size prediction of inclusions is the extreme volume distribution (EVD) method which is based on statistical calculations. By EVD method, the possible maximum size of an inclusion can be estimated in a fixed area/volume [11] with help of ASTM E2283-03 standard [15]. The EVD can be successfully used with help of 2D/3D observation methods [16, 17]. The method is relatively fast, informative and does not require expensive equipment [12, 13]. Another possibility to estimate the probable maximum inclusion's size is a method which is based on the data of particle size distribution (PSD). The PSD prediction method allows to estimate the size of inclusions in the certain volume (weight) of the metal if PSD of inclusions obey to the one specific law. In this study, the PSD prediction method was applied for size distribution of inclusions in steel samples and compared with EVD results.

Since the spherical (SP) inclusions were dominated particles in L/T samples it was decided to estimate a probable maximum size by the PSD and EVD based prediction methods for SP particles.

Prediction based on particles size distribution

The left part of **Fig. 23** shows PSD examples at various magnifications for T10 sample. Usually the PSD is estimated by combination of PSD at different magnifications (high and low) in order to obtain more precise PSD in wide size range. Thereby, it is reasonable to use the same

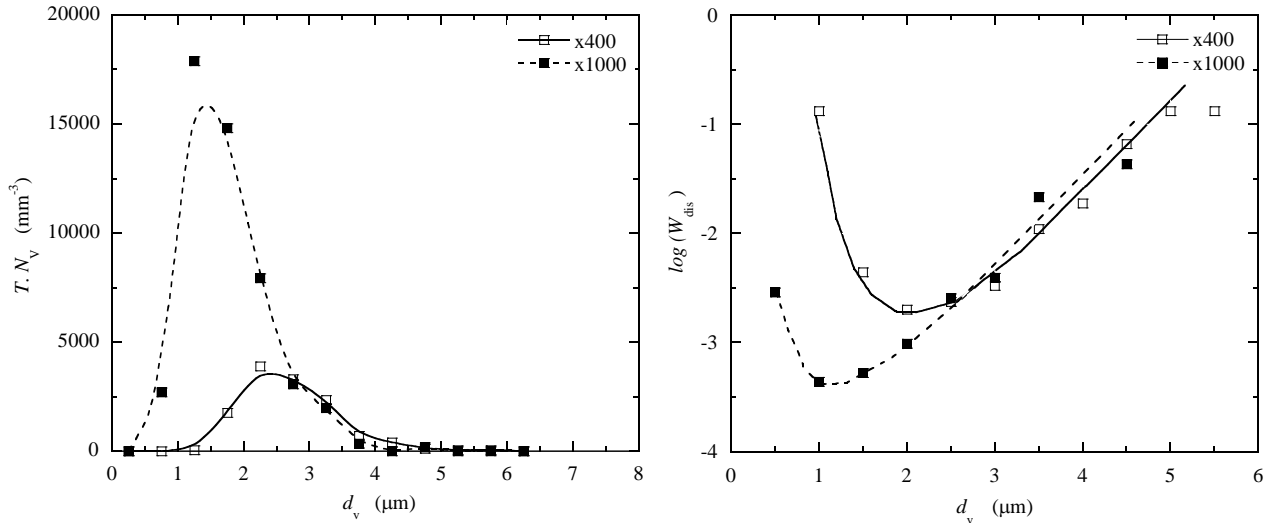


Fig. 23. The particle size distribution for SP particles in T10 sample on the left and the PSD prediction lines in T10 sample on the right.

combination concept for PSD prediction method. The right part of **Fig. 23** shows two PSD prediction lines (0.5 μm size step) at 400 and 1000 magnifications for T10 sample. Since a PSD function complies with a Log-normal function [14] it is possible to obtain the PSD prediction lines with help of Eq.(2).

$$W_{dis(i)} = \frac{\rho_{Me}}{Nv(i)} \quad (2)$$

Where $W_{dis(i)}$ is the weight of steel samples which corresponds to only one inclusion in i -th size range. As can be seen, the PSD prediction lines are close to each other after 2.5 μm which allows to reasonably assume that SP inclusions obey to the same specific law. The part of PSD prediction line at 400 magnification in size smaller than 2.5 μm is not reliable because of measurement accuracy problems for small size inclusions at this magnification and should be neglected. The same neglecting is justified for the PSD prediction line at 1000 magnification in the size less than 1 μm . Since the maximum size prediction estimation is focused on the largest inclusions it is reasonable to use only one low magnification (x400 in this study) but the addition

of higher magnification (x1000) can improve the reliability of prediction data. By the previous assumption the one combined PSD prediction line was calculated. As can be seen in **Fig. 24**, the calculated PSD prediction function correlates well with the experimental data and has high correlation coefficient (R) which in return should provide reliability of prediction data. In the similar manner PSD prediction functions were calculated for SP inclusions in all L/T samples. The calculated PSD prediction functions are summarized in **Table 4**. As can be seen from the table, all prediction function have high R value from 0.97 to 0.99. In addition, the T10 sample has SP inclusions with largest probable maximum size around 15 μm and L10 sample has SP inclusions with smallest probable maximum size around 10 μm corresponding to 1 kg of metal of reference weight.

Table 4. The data for PSD and EVD prediction of the maximum size for SP inclusions in L/T samples for 1 kg of metal.

Sample	Function	R	Size _{max} (μm)
L10*	$y = -5.6203 + 1.1652x$	0.99104	9.97
L40*	$y = -5.5981 + 1.0693x$	0.9889	10.85
L70*	$y = -4.6336 + 0.84731x$	0.99441	12.55
T10*	$y = -4.3993 + 0.69462x$	0.99446	14.97
T40*	$y = -5.1518 + 0.94073x$	0.99583	11.85
T70*	$y = -4.9499 + 0.80459x$	0.97351	13.61
T10**	$y = -10.824 + 3.1188x$	-	9.28

* The PSD method

** The EVD method, y is the calculated regression function

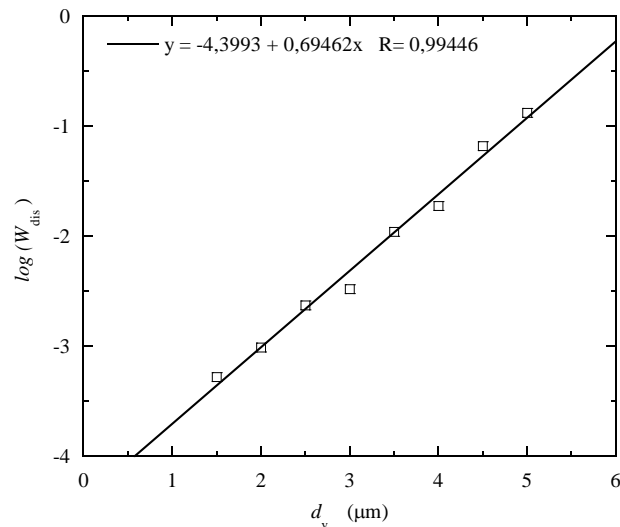


Fig. 24. The PSD prediction line for SP inclusions in T10 sample.

Prediction based on extreme value distribution

In order to check the reliability of the new PSD prediction method it was decided to apply EVD prediction method for maximum size estimation. Since the T10 has the maximum probable size of inclusions it was decided to apply EVD method on the T10 sample. The EVD investigation way is described below:

40 SEM photos were taken at 400 magnification. Unit area (A_0) of each photo is 0.07 mm^2 which in return corresponds with 0,011 mg of dissolved metal. The EVD study was applied with help of Murakami's method [11], ASTM E2283-03 standard [15] and some previous studies in this field [13, 16, 17]. The reference area (A_{ref}) was decided to be equal to 6.2 m^2 which in return corresponds to 1 kg of metal. After involving the y (reduced variate) value (agreed to A_{ref}) the probable maximum size of inclusions can be calculated by Eqs. (3-5) where T is the return period of the area and P is the probability value.

$$y = -\ln\left(-\ln\left(\frac{T-1}{T}\right)\right) \quad (3)$$

$$T = \frac{A_{\text{ref}}}{A_0} \quad (4)$$

$$y = -\ln(-\ln(P)) \quad (5)$$

As can be seen in the left part of **Fig. 25** the calculated regression function (**Table 4**) fits well with experimental data. As a result, it allows to assume that the EVD prediction calculations are reliable. The right part of **Fig. 25** shows the comparison of the PSD and EVD size prediction results for 1 kg of metal. As can be seen, in T10 sample the EVD maximum probable predicted

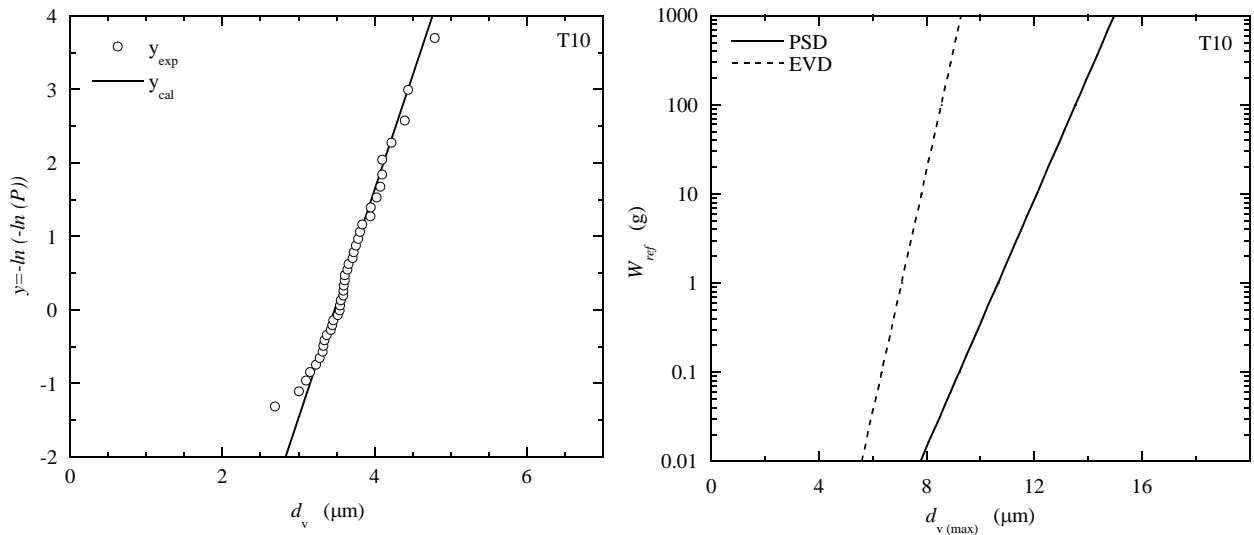


Fig. 25. The EVD regression function on the left. Comparison of prediction PSD and EVD methods for T10 sample on the right.

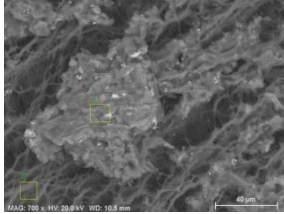
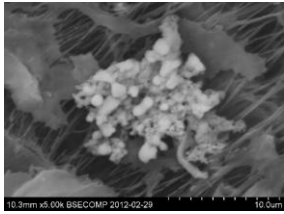
size of SP inclusions is $\sim 9 \mu\text{m}$. Mostly, the difference in prediction results can be caused by the number of inclusions involved in prediction calculations and accuracy of the measurements at different magnifications. For EVD only 40 inclusions were measured but at more “accurate” 4000 magnification. As for PSD method, 243 SP non-metallic particles were included in prediction calculation at both 400 and 1000 magnification. According to the obtained results a further development and optimization of the PSD prediction method is required.

3.2 Characteristic of inclusions in powder forged samples (Set 2)

3.2.1 Morphology of inclusions

The typical observed inclusions in powder forged samples (PF1-PF6) are showed in the **Table 5**. The two main groups are (decreasing in size order): “gray” carbon saturated particles and “bright” clustered inclusions. Since the back scattered electrons signal was applied during SEM observation, it was easy to characterize inclusions by color.

Table 5. The typical morphology and composition of inclusions in PF samples.

Inclusion type	Image	Length (μm)	Chemical composition
“Gray” Carbon saturated (GR)		5 - 250	C-O-Mo-Si-Cr-P-Mg
“Bright” Clustered (BR)		1 - 37	Cr-Si-Mn-Mg-Al-O

3.2.2 Number and size of inclusions

“Gray” carbon saturated particles

The “gray” carbon saturated (GR) particles have the largest L_{max} value (up to $250 \mu\text{m}$). The composition of GR non-metallic particles varies in following range (in wt. %): 61-74% C, 17-25% O, 1-6% Mo, 1-3% Si, 0.2-1.9% Cr, 0.2-0.4% P and 0.1-0.2% Mg. As can be seen, particles have high carbon content. The carbon effect of film-filter’s matrix is low since the inclusions are

quite large in length. The oxygen content is low for considering inclusions like oxides. Thereby, it may be assumed that these particles are graphite particles added into the metal powder before powder forging process or C-compounds precipitations during electrolytic extraction process (actually are not present in steel samples). Namely, during the dissolution of metal matrix a “specific phase” caused by extraction process could separate out.

The PSD (10 μm size step) for GR particles in PF2 sample is showed in **Fig. 26**. The sample has the top of PSD in the range 20-50 μm . The GR particles are not typical non-metallic inclusions in PF samples and the source of these particles is unclear today. In order to obtain more details about these particles more additional investigation is required.

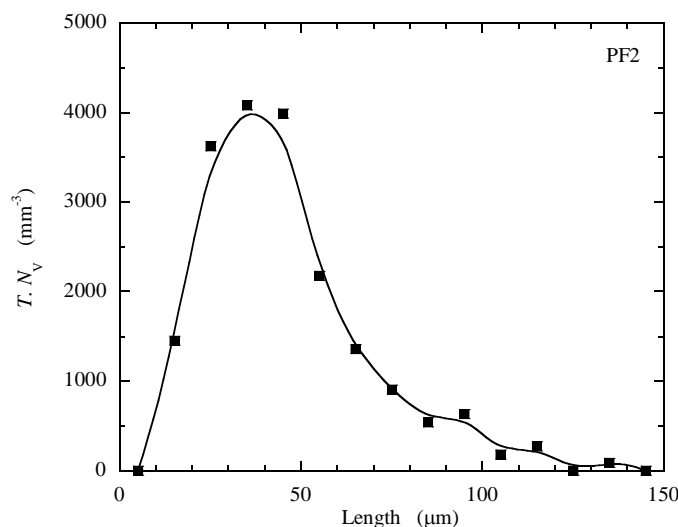


Fig. 26. The PSD of “gray” carbon-saturated particles in PF2 sample.

“Bright” clustered inclusions

“Bright” clustered (BR) inclusions are the second type ($L_{\text{max}} \leq 37 \mu\text{m}$) of non-metallic particles in PF samples. The composition of BR inclusions varies in following range (in wt. %): 23-70% Cr, 35-40% O, 3-11% C, 1-11% Si, 0-11% Mn, 0-2% Mg and 0.1-1.5% Al. The oxygen content is quite high when carbon presence mostly is equal to film-filter’s matrix effect and can be neglected. Based on composition of BR inclusions, it is possible to assume that these particles are unreduced oxide films on metal powder after annealing and particles on metal grains formed during water-atomization.

All PF samples had clear distinguishable BR inclusions. Thereby, PSD of BR inclusions was estimated in all PF samples. The PSD (5 μm size step) for BR particles in PF samples is showed in **Fig. 27**. Only inclusions larger than 4 μm were involved in PSD estimation. All samples have the similar PSD tendencies with the top of PSD in the range $< 7 \mu\text{m}$. However, in this study

the BR inclusions with length $> 40 \mu\text{m}$ were not observed on film-filter after electrolytic extraction.

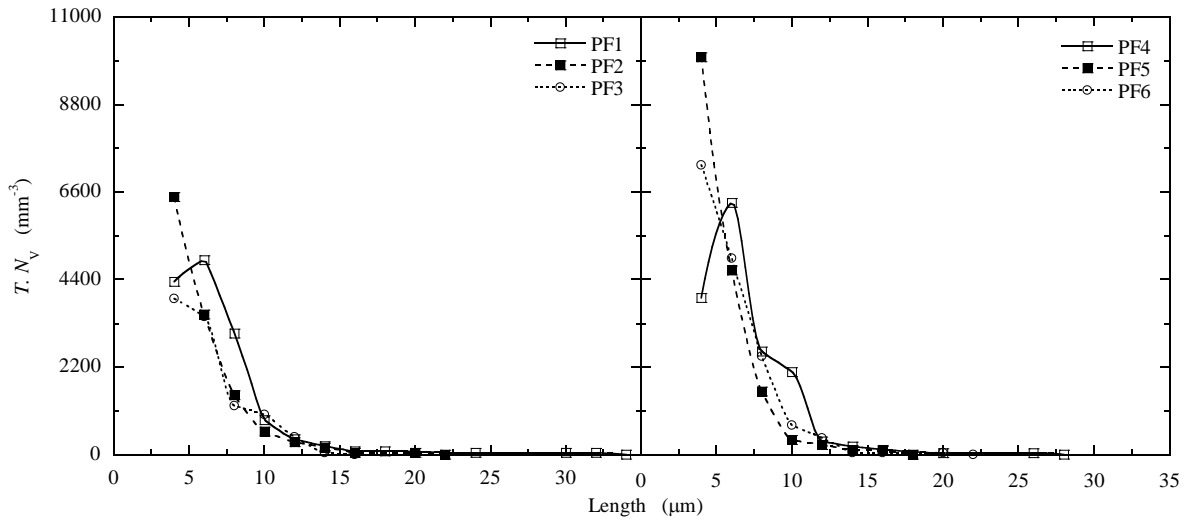


Fig. 27. The PSD of BR inclusions in PF samples.

Based on the assumption about formation of BR inclusions from the residual oxide films, it is reasonable to control oxide films on metal powder carefully in order to prevent probable formation of new inclusions during powder forging process. Anyway, in order to obtain more details about BR particles more investigation is required.

3.2.3 Prediction of the probable maximum size of inclusions

Prediction based on particles size distribution and extreme value distribution

The particle size distribution (PSD) and extreme value distribution (EVD) of for “bright” clustered particles (BR) were applied for prediction of probable maximum size of inclusions in given volume. The prediction functions for each PF samples were calculated in the way described in Sec. 3.1.3. The calculated PSD prediction functions for BR inclusions are summarized in **Table 6**. As can be seen from the table, all prediction functions have high correlation coefficient (R) from ~ 0.96 to ~ 0.97 . The PF4 sample has BR inclusions with maximum probable length around $63 \mu\text{m}$. While, the PF5 sample has BR inclusions with smallest probable length around $42 \mu\text{m}$ corresponding to a reference weight equals to 1 kg of metal. As can be seen in the left part of **Fig. 28**, the calculated regression function (**Table 6**) fits well with the experimental data. As a result, it allows to assume that the EVD prediction calculations are reliable. The right part of **Fig. 28** shows the comparison of the EVD and PSD prediction results for 1 kg of metal. As can be seen, in the PF4 sample the EVD maximum probable predicted length is $60 \mu\text{m}$ which agrees well with the result obtained from PSD method.

The similarity in prediction results can be caused by the number of inclusions involved in prediction calculations. Namely, 40 inclusions were measured for EVD and 61 for PSD prediction estimation which is quite close to each other. Anyway, according to the obtained results a further development and optimization of the PSD prediction method is required.

Table 6. The PSD and EVD prediction of the maximum length for BR inclusions in PF samples for 1 kg of metal.

Sample	Function	R	Length _{max} (μm)
PF1*	$y = -3.8376 + 0.17611x$	0.97838	55.86
PF2*	$y = -3.6604 + 0.17352x$	0.99421	55.67
PF3*	$y = -3.5084 + 0.17815x$	0.96617	53.37
PF4*	$y = -3.6454 + 0.15358x$	0.97826	62.80
PF5*	$y = -4.1212 + 0.24079x$	0.99789	42.03
PF6*	$y = -4.0755 + 0.20482x$	0.99743	49.19
PF4**	$y = -4.646 + 0.38464x$	-	59.68

* The PSD method

** The EVD method, y is the calculated regression function

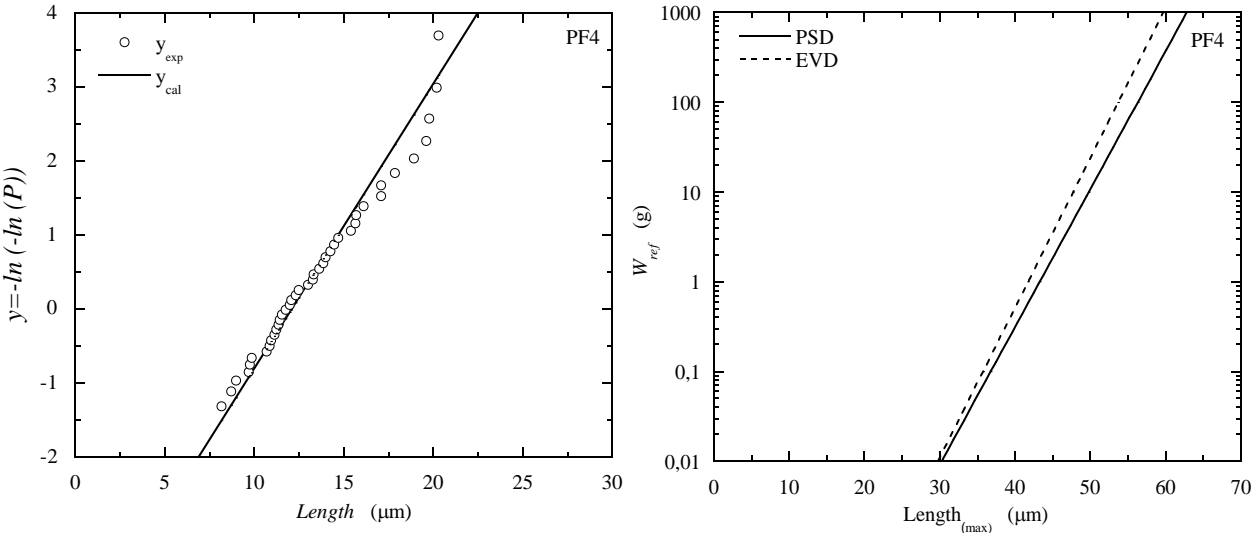


Fig. 28. The EVD regression function on the left. Comparison of prediction PSD and EVD methods for PF4 sample on the right.

4 CONCLUSIONS

The investigation of non-metallic inclusions (NMI) in steel samples taken from different stages of powder metallurgy production (PM) by application of the electrolytic extraction and 3D analysis method (EE-3D) were carried for estimation of the probable maximum size of NMI. The sampling of steel during PM production was performed on industry scale in Höganäs AB. The sampling was made both before water-atomization from the ladle/tundish streams and after powder forging process. The morphology, composition, number, particles size distribution and calculated maximum size of inclusions were estimated for all obtained samples. The particle size distribution (PSD) and extreme value distribution (EVD) prediction methods were applied for estimation of a probable maximum size of inclusions. The final conclusions are following:

- 1) The electrolytic extraction of steel samples can be successfully applied for 3D investigation of NMI in powder metallurgy products.
- 2) The liquid steel samples from the ladle and tundish streams (L10, L40, L70 and T10, T40, T70) have several main types of inclusions: spherical (1-17 μm), elongated (2-20 μm), regular (1-46 μm) and complex (1-25 μm). Most of inclusions (74-92%) in all samples are spherical oxides (composition is Si-Ca-Al-Mg-O). The total number of inclusions in the tundish samples is larger than in the ladle samples due to the reoxidation of liquid steel during the casting.
- 3) The powder forged samples (PF1-6) have two main types of non-metallic particles: “gray” carbon saturated compounds (10-250 μm with C-O (Mo-Si-Cr-P-Mg) in composition and “bright” clustered oxide particles (1-37 μm with Cr-Si-Mn-Mg-Al-O in composition).
- 4) The probable maximum size of spherical inclusions in 1 kg of T10 sample is around 9 μm (EVD method) and 15 μm (PSD method). The probable maximum size of “bright” clustered inclusions in 1 kg of PF4 sample is around 59 μm (EVD method) and 63 μm (PSD method).
- 5) The PSD prediction method can be additionally used for checking prediction results obtained by standard methods.

5 FUTURE WORK SUGGESTIONS

Based on the results of this study, the following is should be done in future work:

- 1) Improvement of the EE method for powder forged samples.
- 2) Studying of the nature behind the “gray” carbon saturated particles in PF samples.
- 3) Application of the EE analysis on the steel powder after water-atomization, annealing, sintering processes.
- 4) Comparison of the results for inclusions characteristics obtained by 2D (cross-section) and 3D (after EE) investigation.
- 5) Improvement of the PSD prediction method.
- 6) Determination and expansion of additional possibilities of EE-3D methods for powder metallurgy products quality analyzing (porosity, voids, fatigue and etc.).

6 REFERENCES

- [1] Reduced Iron Powders Atomized Iron and Steel Powders, JFE Steel Corporation, 2001
- [2] Material and Powder properties, Höganäs AB, 1997
- [3] Höganäs Iron and Steel Powders for Sintered Component, Höganäs AB, 1997
- [4] W. Brian James, “Powder forging”, *Reviews in Particulate Materials*, Vol. 2, 1994, pp.173-214
- [5] A. Petrov, A. Tsipunov, A. Palamarchuk, G. Parabina, et al., “Microdefects in Particles of Atomized High-speed Steel Powders”, *Powder Metallurgy and Metal Ceramics*, Vol. 15, No. 4, 1976, pp. 250-252
- [6] A. Petrov, I. Miroschnichenko, V. Parabin, G. Parabina, et al., “Solidification of Metal Powders During the Atomization of a Liquid Phase”, *Powder Metallurgy and Metal Ceramics*, Vol. 12, No. 1, 1973, pp. 13-16
- [7] A. Karasev., Lectures, *MH2044: Advance Course in Process Science* , KTH, Stockholm, Sweden, 2011
- [8] B. Dogant and T. Davies, ”Fracture Behavior of Powder-forged Steels”, *Industrial and Engineering Chemistry Product Research and Development*, Vol. 25, No. 1, 1986, pp. 72-77
- [9] Seong-Hyeon Hong, Jong-Soo Bae and Yong-Jin Kim, “Effects of Inclusions and Tempering Temperature on The Life of a Powder Compacting Cunch”, *Engineering Failure Analysis*, Vol. 10, 2003, pp. 237–243
- [10] W. James, R. Causton, J. Castelli, T. Murphy, et al., “Microclines Studies of Low Alloy and Carbon Steel, Powders Intended for Powder Forging Applications”, International Powder Metallurgy Conference, Orlando, Florida, 1988
- [11] Y. Murakami, *Metal Fatigue: Effects of Small Defects and Nonmetallic Inclusions*, Tokyo, Japan, 1993
- [12] Y. Kanbe, A. Karasev, H. Todoroki and P. Jönsson, “Application of Statistics of Extreme Values for Inclusions in Stainless Steel on Different Stages of Steel Making Process”, *ISIJ International*, Vol. 51, No. 12, 2011, pp. 2056–2063
- [13] Y. Kanbe, A. Karasev, H. Todoroki and P. Jönsson, “Determination of Inclusions Size Distribution of AISI304 Stainless Steel”, Unpublished research, KTH, Stockholm, Sweden, 2012
- [14] E. Zinngrebe, C. Van Hoek, H. Visser, A. Westendorp, et al., “Inclusion Population Evolution in Ti-alloyed Al-killed Steel during Secondary Steelmaking Process”, *ISIJ International*, Vol. 52, No. 1, 2012, pp. 52–61

[15] ASTM E2283-03, West Conshohocken, PA, American Society for Testing and Materials, 2003

[16] Y. Kanbe, A. Karasev, H. Todoroki and P. Jönsson, “Application of Extreme Value Analysis for Two- and Three-Dimensional Determinations of the Largest Inclusion in Metal Samples”, *ISIJ International*, Vol. 51, No. 4, 2011, pp. 593–602

[17] Y. Kanbe, A. Karasev, H. Todoroki and P. Jönsson, “Analysis of Largest Sulfide Inclusions in Low Carbon Steel by Using Statistics of Extreme Values”, *Steel Research International*. Vol. 82, No. 4, 2011, pp.313-322